NASA TECHNICAL NOTE

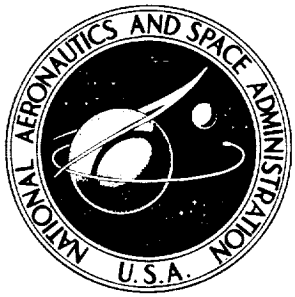

NASA TN D-5440

NASA TN D-5440

POWER- AND CROSS-SPECTRA AND SPACE-TIME CORRELATIONS OF SURFACE FLUCTUATING PRESSURES AT MACH NUMBERS BETWEEN 1.6 AND 2.5

by Wei J. Chyu and Richard D. Hanly

Ames Research Center

Moffett Field, Calif.

NATIONAL AERONAUTICS AND SPACE ADMINISTRATION • WASHINGTON, D. C. • SEPTEMBER 1969

1. Report No. NASA TN D-5440	2. Government Accession No.	3. Recipient's Catalog No.
4. Title and Subtitle POWER- AND CROSS-SPECTRA AND SPACE-TIME CORRELATIONS OF SURFACE FLUCTUATING PRESSURES AT MACH NUMBERS BETWEEN 1.6 AND 2.5		5. Report Date September 1969 6. Performing Organization Code
7. Author(s) Wei J. Chyu and Richard D. Hanly		8. Performing Organization Report No. A-3287
9. Performing Organization Name and Address NASA Ames Research Center Moffett Field, Calif. 94035		10. Work Unit No. 124-08-05-09-00-21 11. Contract or Grant No.
12. Sponsoring Agency Name and Address National Aeronautics and Space Administration Washington D.C. 20546		13. Type of Report and Period Covered Technical Note 14. Sponsoring Agency Code
15. Supplementary Notes		

16. Abstract

A study has been made of the statistical properties of pressure fluctuations that were measured on surfaces adjacent to attached and separated turbulent boundary layers developed on an ogive cylinder and on the cylinder ahead of a 45° cone frustum. Power- and cross-spectra, space-time correlations, convection velocities embracing both broad and narrow frequency bands, and coherence of the pressure field are presented. The pressure field under the attached boundary layer exhibits properties similar to those at subsonic speeds shown by other investigators. Correlations and coherence functions showed a strong dependence on Mach number. Convection velocities are nearly constant with frequency in attached flow, but they vary greatly with frequency in separated flow. Coherence functions are significantly lower in separated flow than under attached boundary layers. Under both attached and separated boundary layers the phase-shift relationship of cospectra and quadspectra is a function of wave number $f\xi_1/U_c(f)$, where f, ξ_1, and U_c represent frequency, spatial distance, and convection velocity, respectively.

17. Key Words (Suggested by Authors)	18. Distribution Statement
Space-time correlations Power- and cross-spectra Convection velocity Turbulent boundary layer (attached and separated) Pressure fluctuation	Unclassified - Unlimited

19. Security Classif. (of this report)	20. Security Classif. (of this page)	21. No. of Pages	22. Price*
Unclassified	Unclassified	19	$3.00

*For sale by the Clearinghouse for Federal Scientific and Technical Information
Springfield, Virginia 22151

POWER- AND CROSS-SPECTRA AND SPACE-TIME CORRELATIONS OF SURFACE FLUCTUATING PRESSURES AT MACH NUMBERS BETWEEN 1.6 AND 2.5[1]

By Wei J. Chyu and Richard D. Hanly

Ames Research Center

SUMMARY

A study has been made of the statistical properties of pressure fluctuations that were measured on surfaces adjacent to attached and separated turbulent boundary layers developed on an ogive cylinder and on the cylinder ahead of a 45° cone frustum. Power- and cross-spectra, space-time correlations, convection velocities embracing both broad and narrow frequency bands, and coherence of the pressure field are presented. The pressure field under the attached boundary layer exhibits properties similar to those at subsonic speeds shown by other investigators. Correlations and coherence functions showed a strong dependence on Mach number. Convection velocities are nearly constant with frequency in attached flow, but they vary greatly with frequency in separated flow. Coherence functions are significantly lower in separated flow than under attached boundary layers. Under both attached and separated boundary layers the phase-shift relationship of cospectra and quadspectra is a function of wave number $f\xi_1/U_c(f)$, where f, ξ_1, and U_c represent frequency, spatial distance, and convection velocity, respectively.

INTRODUCTION

The pressure fluctuations that occur on a surface adjacent to a turbulent boundary layer arise from intricate and unsteady motions of fluid within the boundary layer. The visual observation of the turbulent flows by Runstadler et al. (ref. 1) showed that these unsteady motions are erupted by the intermittent ejections of momentum deficient fluid in the laminar sublayer. However, there is considerable uncertainty as to the origin of these turbulent motions and how they cause the pressure fluctuations.

To study the pressure fluctuations for incompressible flows, Kraichnan (ref. 2) reduced the equations of continuity and motion to an equation of the Poisson type. In this equation the pressure term is dependent on both the turbulence-mean shear and turbulence-turbulence influence. Kraichnan (ref. 2) and Lilley and Hodgson (ref. 3) calculated the power-spectral density under the assumption that the turbulence-mean shear interaction exerts the main influence on the pressure. Although the assumption seems to be justified by a dimensional argument for the boundary layer, the predicted power-spectral density does not agree quantitatively with experimental results. The

[1]This report supersedes AIAA Paper 68-77.

phenomenon of pressure fluctuations viewed mathematically is therefore only vaguely understood, and the approach to the problem has been mainly experimental.

Pressure fluctuations in turbulent incompressible flows have been studied extensively (see, e.g., refs. 4 through 13), but for the case of supersonic attached turbulent flow only a few investigations have been reported (refs. 13-17). In reference 13, Lilley extends the theory developed by Kraichnan to the prediction of the root-mean-square intensity. Measurements of pressure fluctuations under supersonic, separated turbulent flow ahead of a forward-facing step have been reported by Speaker and Ailman (ref. 17), who were concerned primarily with generalization of the experimental data for the use of vehicle designers, and by Kistler (ref. 18), who dealt mainly with the characteristics and mechanism of the pressure field. These investigations are very limited in scope in comparison to the well-documented pressure fluctuations in subsonic flow. Several important statistical functions, such as power spectra, space-time correlations, narrow-band convection velocities, and coherence functions still need to be investigated, particularly in separated flow. These properties are important from the standpoint of improving the understanding of the structure of turbulent flow, and are also necessary for the computation of structural response, fatigue, and interior noise of supersonic flight vehicles.

The unexplored properties of the surface pressure fluctuations in attached and separated turbulent supersonic flows are the focus of the investigation reported in this paper. The study of attached flow is restricted to the case of zero pressure gradient, and the separated flow was generated ahead of a 45° cone frustum. The primary emphasis is on new supersonic data that describe the characteristics and spatial relationship of the pressure fluctuations, convection velocities of the pressure field, and the distinction between these relationships in attached and separated flows.

SYMBOLS

C_f	local skin-friction coefficient
C_p	static-pressure coefficient
$C(\underline{\xi},f)$	cospectral density function
D	diameter of cylinder
f	frequency, Hz
Δf	frequency bandwidth
$G_{\underline{x}}(f)$	power-spectral density function
$G(\underline{\xi},f)$	cross-spectral density function

h	shoulder height of the cone frustum
ℓ	longitudinal distance between the leading edge of the cylinder and the shoulder of the cone frustum
M	Mach number
$\overline{p^2}$	mean square value of pressure fluctuations
$Q(\underline{\xi},f)$	quadspectral density function
q	dynamic pressure
R	Reynolds number
$R_{\underline{x}}(\tau)$	autocorrelation function
$R(\underline{\xi},\tau)$	cross-correlation function
$\overline{T}$	averaging time
t	time
U	velocity in axial direction
U_{CB}	broad-band convection velocity
$U_c(f)$	narrow-band convection velocity
x_s	longitudinal distance measured upstream from the shoulder of the cone frustum
x_1	longitudinal distance measured from the leading edge of the cylinder
x_2	lateral distance measured from the line passing through the longitudinal series of transducers
$\underline{x}(x_1,x_2)$	coordinate referring to location on surface
ξ_1,ξ_2	separation distances of pressure transducers in x_1, x_2 directions
$\underline{\xi}(\xi_1,\xi_2)$	coordinate referring to separation distance of transducers
α	phase angle of cross-spectral density function
γ	coherence function
δ	boundary-layer thickness
δ^*	displacement thickness of boundary layer

θ momentum thickness of boundary layer

τ delay time

τ_w local skin friction

Subscripts

norm normalized quantity

∞ quantity evaluated at free stream

APPARATUS AND TECHNIQUE

Wind Tunnel

Tests were conducted in the Ames 9- by 7-Foot Supersonic Wind Tunnel. The facility is a continuous flow, variable pressure wind tunnel with a stagnation pressure range from 15 to 45 inches Hg. The Mach number is varied by a sliding-block nozzle through a range from 1.55 to 2.6.

Model

Figure 1 is a sketch of the model used for this investigation and illustrates typical flow at supersonic Mach numbers. The 10-inch-diameter ogive cylinder with a 14-inch-diameter axisymmetric ring and 45° cone frustum was used to generate separated turbulent flow upstream of the frustum. The axisymmetric ring and frustum were removed to study attached turbulent flow on the clean ogive-cylinder configuration. A boundary-layer trip of 0.0083-inch-diameter carborundum grit was glued on the ogival nose to assure complete development of an attached turbulent boundary layer.

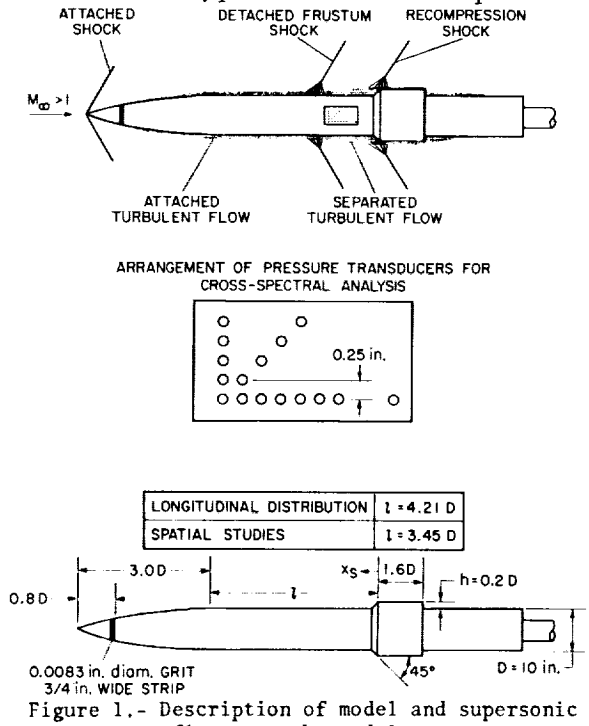

Figure 1.- Description of model and supersonic flow over the model.

Mean Static Pressures

For measurement of static-pressure distributions, the model had approximately 240 pressure orifices distributed over the ogive cylinder, the frustum, and the axisymmetric ring. The pressure measurements were made by standard multiple-port Scanivalve instrumentation

and digital recorder. The static-pressure distributions for attached flow on the ogive-cylinder configuration are not presented in this paper; however, it was observed that there were no pressure gradients over the entire cylinder.

Boundary-Layer Profiles

Mean velocity profiles of both the attached and separated boundary layers were measured with traversing total-pressure probes. Probes were located at x_1/D = 0.2, 0.5, 1.2, and 2.9 to determine the growth of the boundary layer along the cylinder. Mean velocity profiles were obtained at different longitudinal positions in the separated flow by moving the cone frustum (and corresponding region of separated flow) relative to the position of the probe located at x_1/D = 2.9. The velocity profiles were computed from the total pressures and a static pressure adjacent to each probe, using standard equations and assuming no variation existed in static pressure or stagnation temperature across the boundary layer.

Local Skin Friction

Local skin-friction coefficients were calculated from experimental momentum thicknesses by means of equation (25) of reference 19. The calculated local skin-friction coefficients at x_1/D = 2.9 (the region where pressure fluctuations were measured in attached flow) are shown in table I along with corresponding boundary-layer and other flow parameters.

TABLE I.- FLOW PARAMETERS FOR ATTACHED TURBULENT FLOWS

M_∞	U_∞, fps	q_∞, psf	$R\times10^{-6}$ per ft	δ, in.	δ^*, in.	θ, in.	$C_f\times10^3$
1.6	1536	895	3.93	0.612	0.125	0.055	2.00
2.0	1751	760	3.48	.618	.142	.047	1.95
2.5	1942	543	2.79	.635	.155	.040	1.88
				Evaluated at x_1/D = 2.9			

Static-Pressure Fluctuations

Transducers and installation.- The static-pressure fluctuations were measured by 0.125-inch-diameter differential pressure transducers. The transducers, which utilize semiconductor strain gages for detection of pressure, were mounted with the pressure-sensing diaphragms flush with the model surface. The reference pressure tube on the back of each transducer was connected to an adjacent static-pressure orifice through a coil of approximately 10 feet of 0.025-inch I.D. tubing. The length and size of tubing was selected so that the attenuation of fluctuations in the reference pressure would exceed 95 percent at frequencies above 10 Hz. The transducers were

spaced longitudinally between $x_1/D = 2.8$ and 4.0 on the 10-inch-diameter cylinder and on the cone frustum to obtain the overall distributions. A group of closely spaced transducers was also oriented about $x_1/D = 2.9$ for the longitudinal and lateral spatial correlation measurements (fig. 1). The shoulder of the cone frustum was located at $l = 4.21$ D for measurement of the overall distributions, and at $l = 3.45$ D for the space-time correlation studies.

Related instrumentation.- The transducers were individually powered by dc voltage supplies, and the output signals were amplified by single-ended dc amplifiers. The resulting voltage time histories were tape recorded at a speed of 60 in./sec. Frequency modulation, with center carrier frequencies of 108 kHz, was used in the recording to achieve flat frequency response from 0 to 20 kHz. High-pass filters, which attenuated the voltage 3 dB at approximately 5 Hz, could be switched into or out of the electrical circuits between the amplifiers and the tape recorder. When fluctuating-pressure data were recorded, the filtering was applied to eliminate the recording of dc voltage variations.

Transducer calibrations.- The high-pass filters were switched out of the electrical circuit to take advantage of the zero-frequency-response capability of the system for pressure sensitivity calibrations. Daily checks of the transducer sensitivities were made by applying ±1 psi gage pressures through the reference pressure tubing. Laboratory checks of the transducers prior to model installation showed that thermal effects on the sensitivity could be expected to be less than 2 percent for the temperature range of the tests.

Frequency response of transducers.- The frequency-response capability of the transducers is considered to be acceptably flat up to 20 kHz. Natural frequencies of the transducers ranged from 60 to 90 kHz. Frequency-response calibrations have not been applied to 20 kHz. However, the damping of the response of the transducer diaphragm-strain-gage combination was found to be less than 10 percent of critical damping. The frequency response would therefore be expected to be within 1 dB of flat response at 20 kHz, and phase errors due to mismatching of the phase shift between applied pressure and voltage output at 20 kHz would be expected to be negligible.

Transducer size corrections.- Corrections to account for the finite area of the pressure-sensing diaphragm of the transducers were applied to the power spectra of the pressure fluctuations in attached flow. The method derived by Corcos et al. (ref. 20) was used. No corrections were applied to the data obtained in separated flow.

Data reduction.- The definitions and methods for acquisition of the statistical functions used to describe the properties of random pressure fluctuations are briefly summarized below:

1. Root-mean-square pressure. The rms values of the pressure fluctuations defined by $\overline{p^2} = \int_0^\infty G(f)df$ were obtained by integrating the power-spectral-density functions over the frequency range from 10 Hz to 20 kHz.

The results were checked with values obtained from rms meter readings. The rms values were made dimensionless by dynamic pressure and by skin friction.

2. Power- and cross-spectra. The power- and cross-spectral densities in the frequency range from 10 Hz to 20 kHz were obtained by a hybrid analog-digital computing process (ref. 21) for a total of 106 frequency points per spectrum measurement. They are defined as follows:

a. Power-spectral-density function

$$G_{\underline{x}}(f) = \lim_{\substack{\Delta f \to 0 \\ \overline{T} \to \infty}} \frac{1}{(\Delta f)\overline{T}} \int_0^{\overline{T}} p_{\underline{x}}^2(t;f,\Delta f)dt$$

where $p_{\underline{x}}(t)$ denotes time history record of pressure fluctuations measured at location $\underline{x}$; and $p(t;f,\Delta f)$ is that portion of $p(t)$ in a frequency range from $f - \Delta f/2$ to $f + \Delta f/2$.

b. Cross-spectral-density function

$$G(\underline{\xi},f) = C(\underline{\xi},f) - jQ(\underline{\xi},f)$$

where the cospectral density C and quadspectral density Q are defined as

$$C(\underline{\xi},f) = \lim_{\substack{\Delta f \to 0 \\ \overline{T} \to \infty}} \frac{1}{\Delta f \overline{T}} \int_0^{\overline{T}} p_{\underline{x}}(t;f,\Delta f)p_{\underline{x}+\underline{\xi}}(t;f,\Delta f)dt$$

and

$$Q(\underline{\xi},f) = \lim_{\substack{\Delta f \to 0 \\ \overline{T} \to \infty}} \frac{1}{\Delta f \overline{T}} \int_0^{\overline{T}} p_{\underline{x}}(t;f,\Delta f)p^0_{\underline{x}+\underline{\xi}}(t;f,\Delta f)dt$$

$p^0_{\underline{x}+\underline{\xi}}(t;f,\Delta f)$ denotes a 90° phase shift from $p_{\underline{x}+\underline{\xi}}(t;f,\Delta f)$. In the normalized form,

$$C(\underline{\xi},f)_{norm} = \frac{C(\underline{\xi},f)}{\left[G_{\underline{x}}(f)G_{\underline{x}+\underline{\xi}}(f)\right]^{1/2}}$$

and

$$Q(\underline{\xi},f)_{norm} = \frac{Q(\underline{\xi},f)}{\left[G_{\underline{x}}(f)G_{\underline{x}+\underline{\xi}}(f)\right]^{1/2}}$$

The computing procedure applied corrections for phase errors introduced by misalinement of the tape-recorder record and reproduce heads. The frequency bandwidth Δf and the average time $\overline{T}$ imposed on the analog during the spectrum measurements are given in table II. The normalized standard errors in the estimation of power- and cross-spectral-density function, approximated by $\varepsilon \approx 1/\sqrt{\Delta f \overline{T}}$ (ref. 22), are also tabulated in table II.

TABLE II.- OPERATING PARAMETERS FOR THE HYBRID ANALOG-DIGITAL ANALYSIS OF POWER- AND CROSS-SPECTRA

Frequency range, Hz	Frequency bandwidth, Δf, cps	Average time, $\overline{T}$, sec	Number of frequency points	Normalized standard errors of power- and cross-spectral densities, percent
10-50	2	20	21	15.8
60-240	10	20	19	7.0
260-1,020	40	10	20	5.0
1,200-5,200	200	2	21	5.0
5,600-10,400	400	2	13	3.5
11,200-20,000	800	2	12	2.5

3. Correlation functions. The auto- and cross-correlation functions are defined as:

a. Autocorrelation:

$$R_{\underline{x}}(\tau) = \lim_{\overline{T}\to\infty} \frac{1}{\overline{T}} \int_0^{\overline{T}} p_{\underline{x}}(t)p_{\underline{x}}(t+\tau)dt$$

b. Cross-correlation:

$$R(\underline{\xi},\tau) = \lim_{\overline{T}\to\infty} \frac{1}{\overline{T}} \int_0^{\overline{T}} p_{\underline{x}}(t)p_{\underline{x}+\underline{\xi}}(t+\tau)dt$$

In this paper, the correlation functions were obtained by applying an inverse Fourier transform to power- and cross-spectral-density functions:

$$R_{\underline{x}}(\tau) = \int_0^{\infty} G_{\underline{x}}(f)\cos 2\pi f\tau \, df$$

and

$$R(\underline{\xi},\tau) = \int_0^\infty [C(\underline{\xi},f)\cos 2\pi f\tau + Q(\underline{\xi},f)\sin 2\pi f\tau]df$$

In the normalized form,

$$R_{\underline{x}}(\tau)_{norm} = \frac{R_{\underline{x}}(\tau)}{R_{\underline{x}}(0)}$$

and

$$R(\underline{\xi},\tau)_{norm} = \frac{R(\underline{\xi},\tau)}{R(\underline{\xi},0)}$$

RESULTS AND DISCUSSION

Root Mean Square of Pressure Fluctuations

The effects of Mach number on root-mean-square intensities of the pressure fluctuations in attached flows, made dimensionless by q_∞, are shown in figure 2. The results of this investigation, while limited in Mach number range, are within the spread of data from other investigators. The rms value of pressure fluctuations varied from $\sqrt{\overline{p^2}} = 0.004\ q_\infty$ to $0.002\ q_\infty$ as the Mach number was increased from 1.6 to 2.5. However, if the same rms data are made dimensionless using local skin friction, the result is an inconsistent variation with Mach number. No definite explanation was found for this discrepancy of $\sqrt{\overline{p^2}}/\tau_w$ for supersonic flows, but it no doubt is associated with the inaccurate predictions of the local skin friction, and the possibility that skin friction is associated only with the high-frequency components of the overall pressure fluctuations.

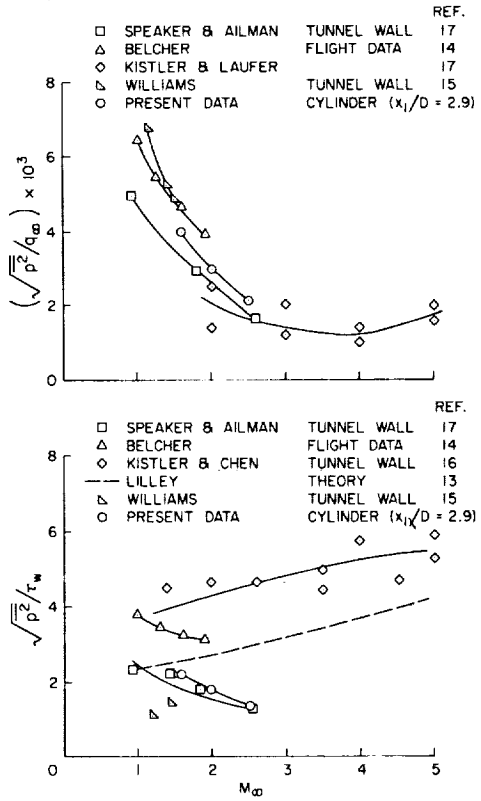

Figure 2.- Mach number on root-mean-square pressure fluctuation in attached flow.

The longitudinal variations of velocity profiles, mean static pressures, and fluctuating pressures on the surface of the cylinder ahead of the cone frustum are shown in figures 3 and 4. These figures illustrate characteristic features of the

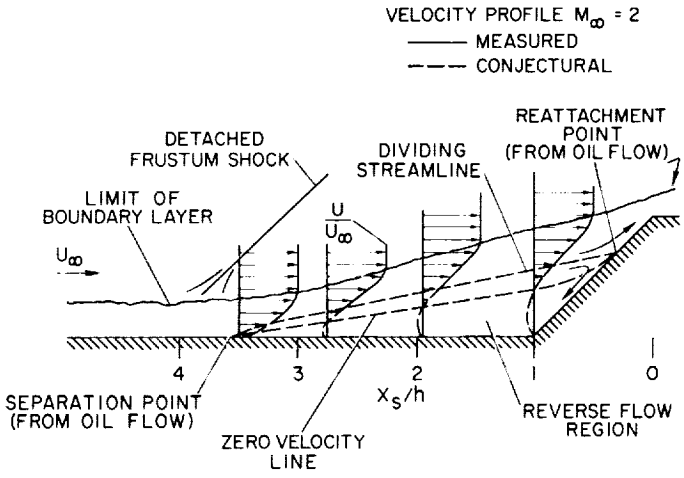

Figure 3.- Separated turbulent flow ahead of cone frustum.

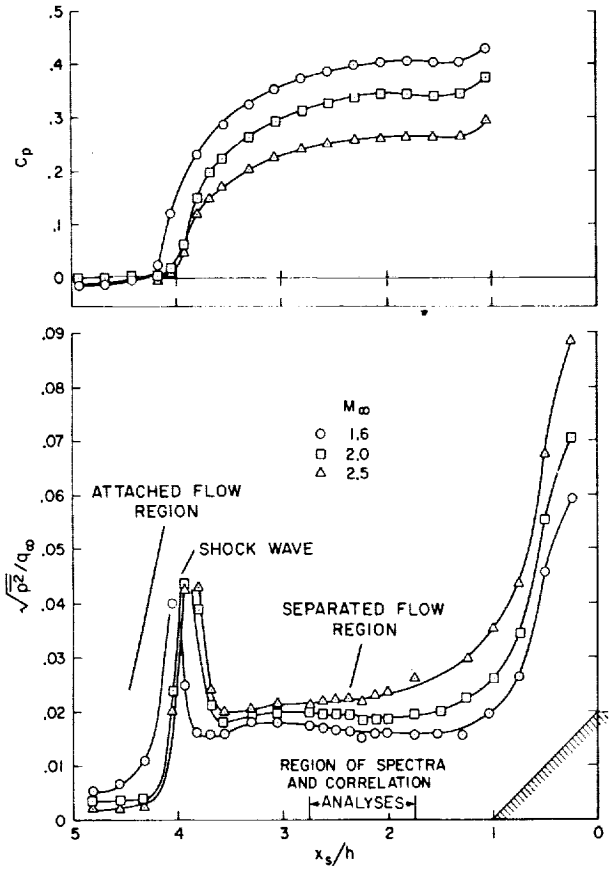

Figure 4.- Longitudinal variation of steady and fluctuating pressure in separated turbulent flow.

flow in the vicinity of separation and locally where the spectra and correlation analyses were conducted. The static pressure, initially at the free-stream value, increases rapidly as the flow encounters the detached frustum shock wave near the separation point; it then slowly approached a plateau as the transition from the attached to the separated flow is completed. After the plateau is reached, the pressure starts to increase immediately ahead of the cone frustum. This trend is similar to the results obtained by Chapman et al. (ref. 23). Characteristic features of the pressure fluctuations can be related to features of the static-pressure distribution. The pressure fluctuations increase rapidly at the shock wave, reaching a maximum $\left(\sqrt{\overline{p^2}}/q_\infty \approx 0.05\right)$ at the point of inflection in the static-pressure curve. In the fully separated region, the fluctuating pressure descends to a plateau level corresponding to the plateau region of the static-pressure distribution. Immediately ahead of the frustum and on the frustum, the pressure fluctuations rapidly increase, an effect caused by the abrupt geometrical change of the surface. The level of the pressure fluctuations in the separated region is significantly larger than that in the attached flow region.

Longitudinal-Cross-Spectral Density and Coherence Functions

The in-phase and out-of-phase components of two time-history records of pressure fluctuations

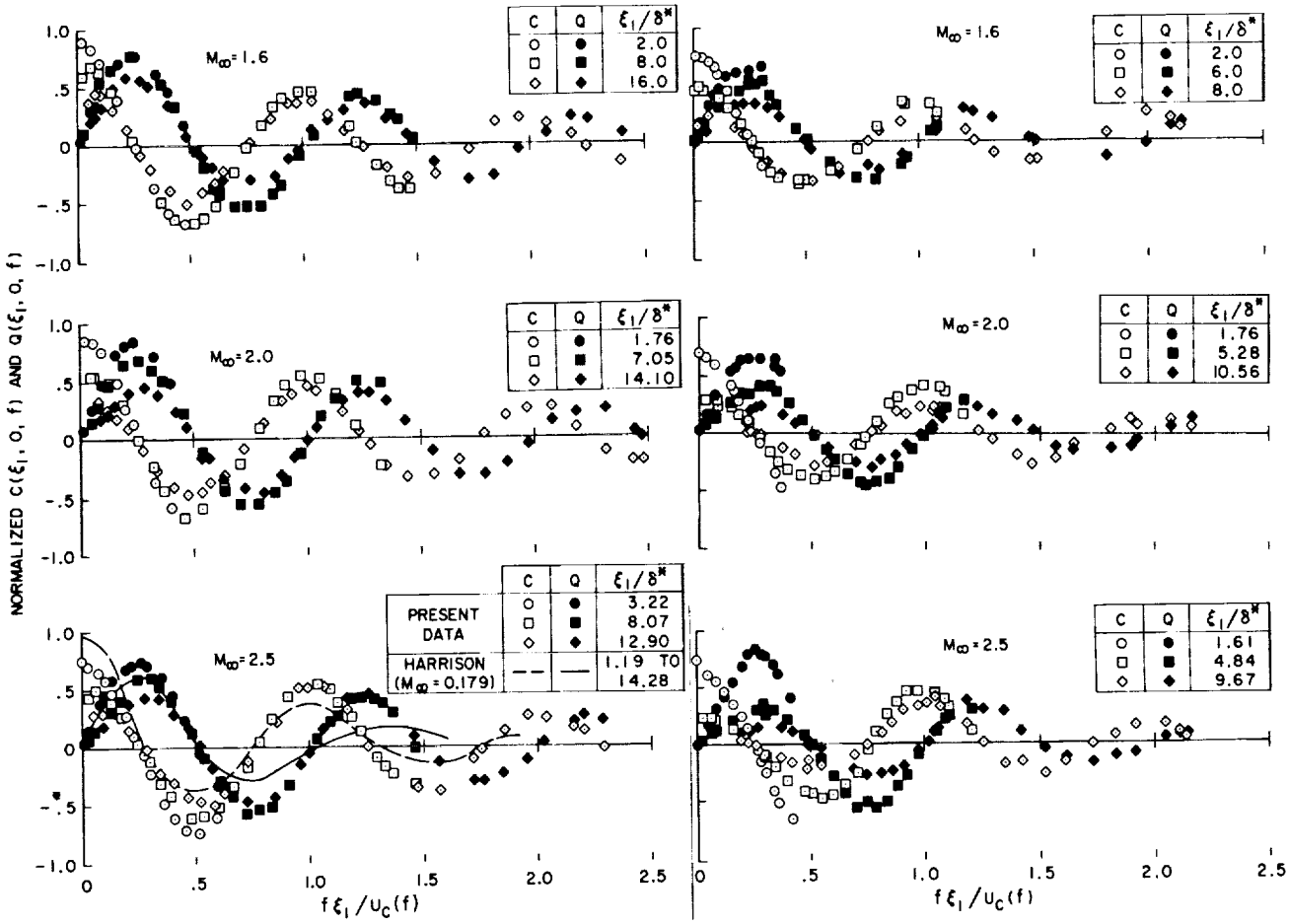

(a) Attached flow. (b) Separated flow.

Figure 5.- Longitudinal cross spectra of pressure fluctuations.

can be described by cospectral and quadspectral density functions. Figure 5 shows normalized cross-spectra plotted against the wave-number parameter $f\xi_1/U_c(f)$ for various separation distances in the longitudinal direction. Harrison (ref. 8) applied the parameter $f\xi_1/U_\infty$ to subsonic attached flow at $M_\infty = 0.179$; this investigation showed that it can also be applied to both attached and separated supersonic flows, provided the velocity term is the narrow-band convection velocity instead of the free-stream velocity. The cross-spectra can be represented by damped sinusoidal waves, which can be interpreted as a loss of identity of turbulent eddies and the development of uncorrelated components as the eddies convect downstream.

The component of the power spectrum of the downstream pressure that is correlated to the upstream pressure can be depicted by the coherence function $\gamma(\underline{\xi},f) = |G(\underline{\xi},f)|^2/|G_{\underline{x}}(f)||G_{\underline{x}+\underline{\xi}}(f)|$, which is plotted in figure 6 as a function of $f\xi_1/U_c(f)$. The envelope of the coherence functions for various spatial distances ξ_1/δ^* decreases exponentially with increasing wave number. For a given ξ_1/δ^*, the coherence can be represented by the envelope only at

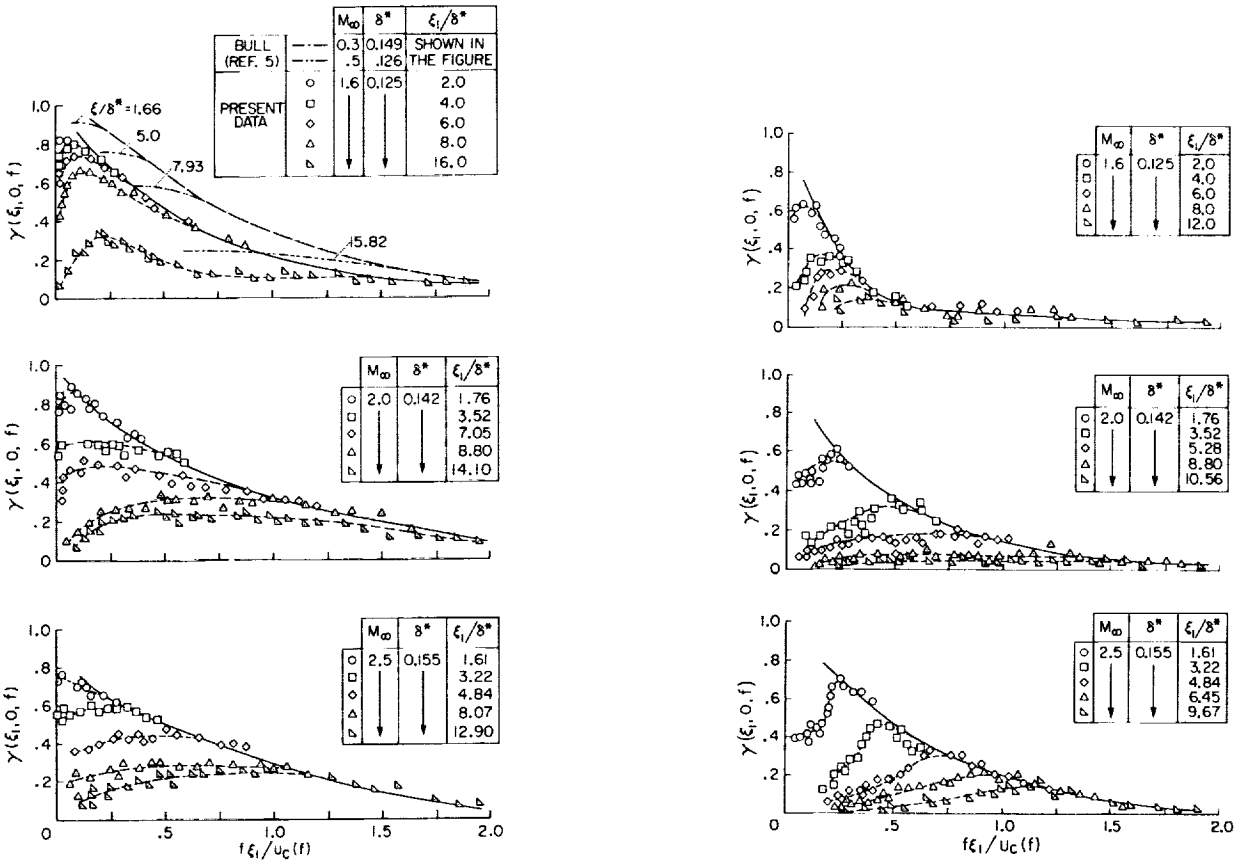

(a) Attached flow. (b) Separated flow.

Figure 6.- Longitudinal coherence of pressure fluctuations.

high frequencies, the lower limits of which increase with increasing distance between transducers. The envelope approaches unity as $f\xi_1/U_c(f) \to 0$ or $\xi_1 \to 0$ at finite f. Bull (ref. 5) showed that it is physically impossible for the coherence to approach unity if $f \to 0$ at finite ξ_1, since in that case low-frequency components of the wall pressure would be coherent over infinite distance. For a given ξ_1/δ^*, the coherence at low frequency decreases with increasing Mach number, whereas the coherence at high frequency increases. The variation of the envelope with Mach number is more significant in the separated flow than in attached flow, with higher frequencies becoming better correlated as Mach number is increased. The coherence also decreases more rapidly with increasing spatial distance and frequency in separated flow than in attached flow.

Correlation Functions

The space-time correlation between two time-history records of pressure fluctuations can be described by the cross-correlation functions. Figure 7 shows the normalized correlation functions plotted against time τ for various longitudinal separation distances measured from the transducer location $x_1/D = 2.9$. The decrease of the peak of the correlations with

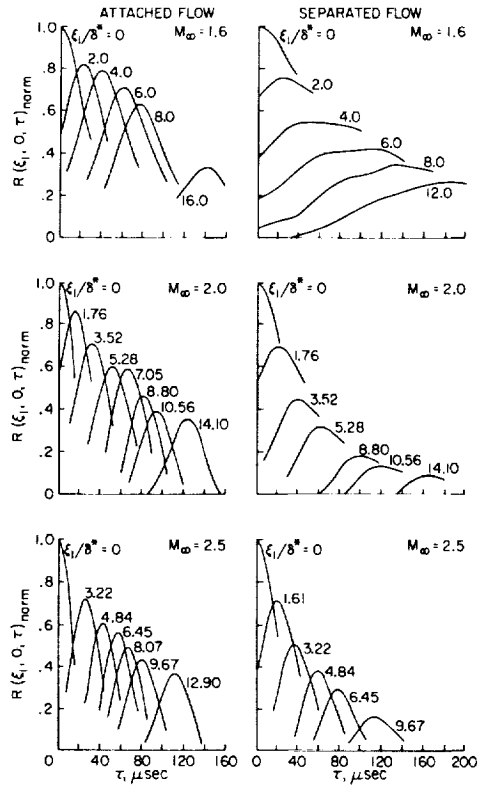

Figure 7.- Longitudinal space-time correlation of pressure fluctuations.

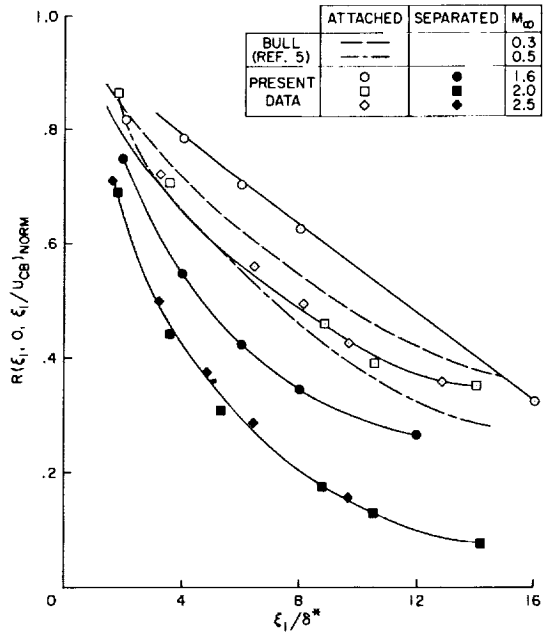

Figure 8.- Longitudinal space correlations in attached and separated flows. Space-time correlations, $R(\xi_1, 0, \tau)$ at time delay, $\tau = \xi_1/U_{CB}$ or at the peaks of curves in figure 7.

increasing ξ_1 indicates the decay of the turbulent eddies as they travel downstream. For a given Mach number the correlation curves broaden with increasing separation distance ξ_1, which indicates that the decay of the low-frequency turbulent eddies is not as rapid as that of high-frequency eddies.

For a given ξ_1/δ^*, the correlation curves tend to sharpen with increased Mach number. This implies that the longitudinal correlation of the high-frequency turbulent eddies become more predominant with the increasing Mach number, as also was observed in the coherence functions.

For a given ξ_1/δ^* and M_∞, the correlation curves in the attached flow are significantly sharper than those in the separated flows, indicating that the correlation in the attached flow is due to turbulent eddies whose frequencies are higher than the eddies in the separated flow.

Figure 8 shows the longitudinal spatial correlations obtained when the space-time correlations are referred to coordinates moving with the corresponding average convection velocity of the turbulent eddies, and peak correlation magnitudes at corresponding convection times ξ_1/U_{CB} are plotted against the separation distance ξ_1/δ^*. The result indicates that the longitudinal spatial correlation in the attached flow was significantly higher than that in the separated flow, and also that the effect of the Mach number on the spatial spatial correlations was significant for $1.6 < M_\infty < 2.0$ but negligible for $2.0 < M_\infty < 2.5$.

As shown in figure 9, lateral spatial correlations, for the attached flows were independent of the Mach number, whereas those for the separated flows decreased with the increasing Mach number.

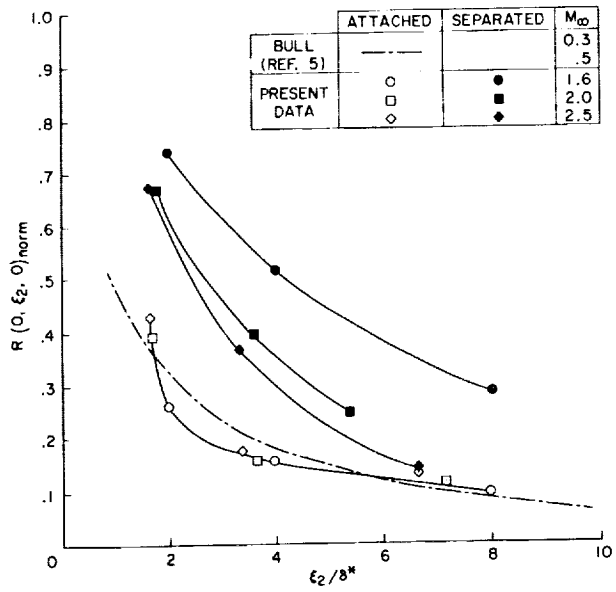

Figure 9.- Lateral space correlation of pressure fluctuations in attached and separated flows.

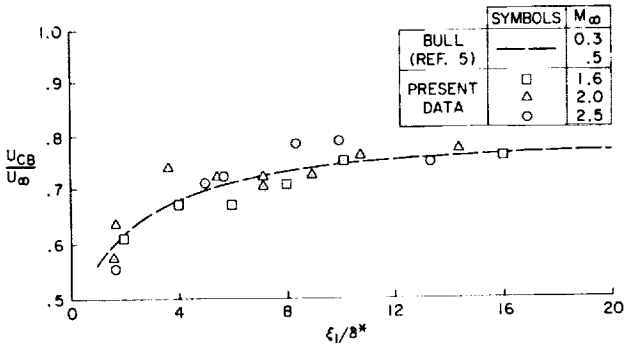

Figure 10.- Variation of broad-band convection velocity with separation distance in attached flow.

Comparison of attached-flow longitudinal and lateral spatial correlations (figs. 8 and 9) with Bull's data (ref. 5) indicates that the correlation and decay of turbulence with distance are similar for both subsonic and supersonic flows.

Convection Velocity of Pressure Field

A broad-band convection velocity is defined as the quotient of the separation distance of transducers and the time delay at the peak of the cross-correlation. It represents the average velocity of the turbulent eddies that contribute most to the production of wall-pressure fluctuations. Figure 10 shows the broad-band convection velocity of the pressure field in the attached flows as a function of separation distance ξ_1/δ^*. The increase of the convection velocity from 0.55 U_∞ to 0.8 U_∞ with increasing ξ_1/δ^* implies an outward dispersion of the turbulent eddies from the lower speed inner layers of the boundary layer. This is the type of flow visually observed in subsonic flow by Runstadler et al. (ref. 1). The present measurements compare favorably with the subsonic results of Bull (ref. 5).

A narrow-band convection velocity defined by $2\pi f\xi_1/\alpha(\xi_1,f)$ (where $\alpha(\xi_1,f) = \tan^{-1}[Q(\xi_1,f)/C(\xi_1,f)]$) represents the convection velocity of a turbulent eddy traveling downstream with frequency f. Figure 11 shows the representative convection velocities as a function of $f\xi_1/U_\infty$.

For the attached flows, the convection velocities were constant for frequencies above 5 kHz and were closely approximated by the broad-band convection velocity. At frequencies below 5 kHz, the convection velocity approaches unity. These results indicate that the higher frequency components of the wall-pressure fluctuation must be caused by the turbulent eddies prevailing near the wall, and that the lower frequency components were caused by the turbulent eddies in the outer region of the boundary layer and/or by free-stream turbulence. Since these trends agree with the visual observations (ref. 1) for subsonic flow, it can be concluded that the mechanism of

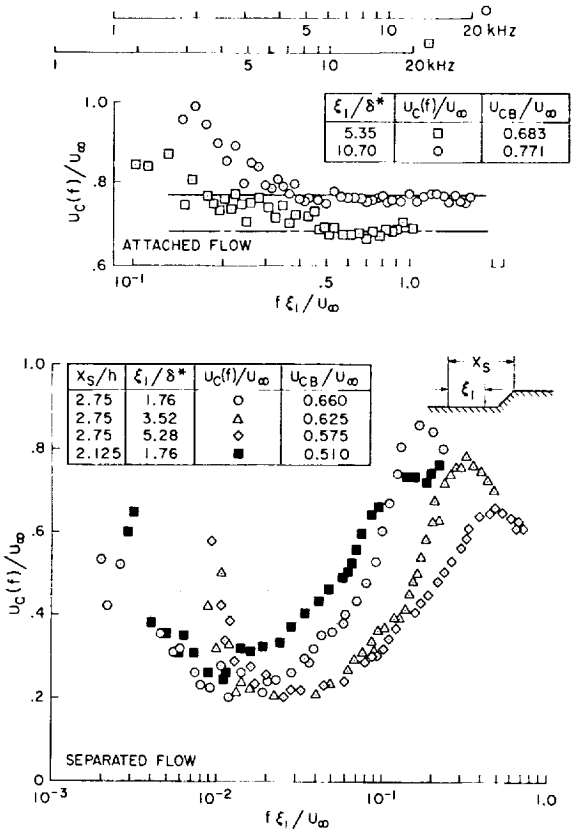

Figure 11.- Narrow-band convection velocity of pressure field at $M_\infty = 2.0$.

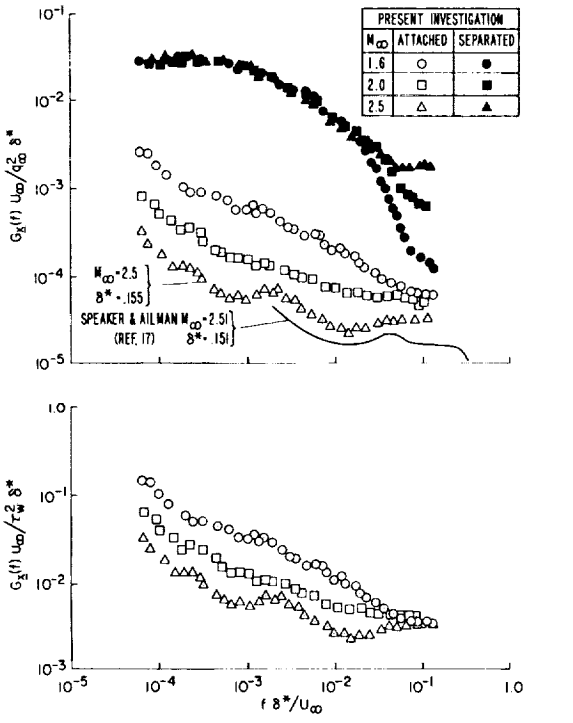

Figure 12.- Power spectra of pressure fluctuations.

the turbulence in a turbulent boundary layer in supersonic flow is the same as in subsonic flow.

For the separated flows, the narrow-band convection velocities shown in figure 11 vary approximately from $0.2\ U_\infty$ to $0.8\ U_\infty$ within the frequencies investigated. Thus, broad-band convection velocities as determined from cross-correlation functions cannot be considered representative. The variation of the convection speed, when related to the boundary-layer profiles shown in figure 3, indicates that the primary source of the wall-pressure fluctuations exists in the high shear-force region from near the zero-velocity line to the free-shear layer. Since negative convective velocities were not detected, turbulent eddies in the reverse flow region apparently contribute little to the wall-pressure fluctuations.

Power-Spectral Density

The frequency content of the pressure fluctuations by the power-spectral density functions is shown in figure 12 for both attached and separated flows. Only the data measured at $x_1/D = 2.9$ are presented; however, they are representative of the power spectra measured over most of the separated region.

The power spectra for the attached flows show a trend similar to results obtained by Speaker and Ailman (ref. 17) within the same frequency range investigated. Their data were chosen for comparison because their aerodynamic parameters, shown in figure 12, best approximated those of the present investigation. If the same power-spectral density for the attached flows are nondimensionalized with local skin friction instead of q_∞, a somewhat closer similarity of the power

spectra for all the Mach numbers is obtained for $f\delta^*/U_\infty > 0.04$. The similarity at high frequencies supports the argument that the turbulence of small high-frequency eddies is dominated by viscous forces that exist near the wall where the local skin friction exerts the major influence.

In the case of separated flow, the power spectral densities were made dimensionless by the displacement thickness ahead of the separation point. The power spectra show that the pressure fluctuations were significantly higher than in the attached flow, as was seen in the root-mean-square curve. The high pressure fluctuations arise indirectly from the shear force necessary to counterbalance the momentum directed to the cone frustum. This is inferred from the fact that the convection velocity $U_c(f)$ of the pressure field varies from $0.2\ U_\infty$ to $0.8\ U_\infty$ in the frequency range investigated. The power spectra, made dimensionless by q_∞, collapsed into a single curve at reduced frequencies $f\xi^*/U_\infty < 0.02$. For $f\xi^*/U_\infty > 0.02$, the power spectra increased with increasing Mach number. The convection velocity $U_c(f)$ of the turbulent eddies that predominates the power spectra at $f\xi^*/U_\infty < 0.02$ is approximately $0.8\ U_\infty$. Therefore, these turbulent eddies must prevail where the local flow is supersonic; hence they are sensitive to the variation of Mach number.

CONCLUSIONS

The study of statistical properties of pressure fluctuations measured on surfaces adjacent to attached and separated turbulent boundary layers disclosed the following:

1. The spatial relationship of the fluctuating pressures in attached supersonic flow, such as cospectra and quadspectra, coherence functions, cross-correlation functions, and broad-band convection velocities, is similar to that shown by other investigators for subsonic flow.

2. Root-mean-square pressure fluctuations in attached flow made dimensionless by dynamic pressure varied from 0.004 to 0.002 as Mach number was increased from 1.6 to 2.5.

3. The cospectra and quadspectra of pressure fluctuations in the longitudinal direction can be expressed as a function of wave number for both attached and separated flow. The cross-spectra in this form appear as damped sinusoidal waves.

4. The coherence function, expressed as a function of wave number, represents the sum of the squares of the normalized cospectra and quadspectra. The envelopes for both attached and separated flows approach unity as spatial distance of transducers approaches zero at finite frequency. The coherence departs from this envelope at low frequency, indicating that the decay of coherence with spatial distance is affected more at low frequencies than at high frequencies.

5. The longitudinal spatial correlation of the pressure field referring to the coordinates moving with the corresponding convection velocity shows that the correlation in the attached flow is significantly higher than that in the separated flow.

6. For supersonic attached flow, the convection velocity as a function of frequency was constant at frequencies above 5 kHz and could be closely approximated by the broad-band velocity. At frequencies below 5 kHz, the convection velocity approached unity. These results indicate that the higher frequency components of the wall-pressure fluctuation must be caused by the turbulent eddies prevailing near the wall, and that the lower frequency components were caused by the turbulent eddies in the outer region of the boundary layer and/or by free-stream turbulence.

7. The variation of convection velocity with transducer separation distance in attached flow indicates an outward dispersion of turbulent eddies from inner layers of the boundary layer.

8. Convection velocities in supersonic separated flow vary greatly with frequency, and thus the broad-band convection velocity as determined from cross-correlation functions cannot be regarded as being representative.

9. The narrow-band convection velocities indicate that the main source of the wall-pressure fluctuations in separated flow is in the high-shear flow region in the stream direction. Since reverse convection was not detected, turbulent eddies in the reverse flow region apparently contribute little to the surface-pressure fluctuations.

Ames Research Center
National Aeronautics and Space Administration
Moffett Field, Calif., 94035, June 26, 1969

REFERENCES

1. Runstadler, P. W.; Kline, S. J.; and Reynolds, W. C.: An Experimental Investigation of the Flow Structure of a Turbulent Boundary Layer. AFOSR-TN-5421, June 1963.

2. Kraichnan, R. H.: Pressure Fluctuations in the Turbulent Flow Over a Flat Plate. J. Acoust. Soc. Am., vol. 28, 1956, p. 378.

3. Lilley, G. M.; and Hodgson, T. H.: On Surface Pressure Fluctuations in Turbulent Boundary Layers. AGARD Rep. 276, April 1960.

4. Bakewell, H. P., Jr.; Carey, G. F.; Libuha, J. J.; Schlormer, H. H.; and von Winkle, W. A.: Wall Pressure Correlations in Turbulent Pipe Flows. U.S. Navy Underwater Sound Laboratory Rep. 559, Aug. 1962.

5. Bull, M. K.: Wall-Pressure Fluctuations Associated With Subsonic Turbulent Boundary Layer Flow. J. Fluid Mech., vol. 28, pt. 4, 1967, p. 719.

6. Bull, M. K.; and Willis, J. L.: Some Results of Experimental Investigations of the Surface Pressure Field Due to a Turbulent Boundary Layer. A.A.S.U. Rep. 199, Nov. 1961.

7. Corcos, G. M.: The Structure of the Turbulent Pressure Field in Boundary-Layer Flows. J. Fluid Mech., vol. 18, pt. 3, 1964, p. 353.

8. Harrison, M.: Pressure Fluctuations on the Wall Adjacent to a Turbulent Boundary Layer. David Taylor Model Basin Rep. 1260, Dec. 1958.

9. Serafini, J. S.: Wall-Pressure Fluctuations and Pressure Velocity Correlations in a Turbulent Boundary Layer. NASA TR R-165, 1963.

10. Shattuck, R. D.: Sound Pressures and Correlations of Noise on the Fuselage of a Jet Aircraft in Flight. NASA TN D-1086, 1961.

11. Willmarth, W. W.: Space-Time Correlations and Spectra of Wall Pressure in a Turbulent Boundary Layer. NASA MEMO 3-17-59W, 1959.

12. Willmarth, W. W.; and Wooldridge, C. E.: Measurements of the Fluctuating Pressure at the Wall Beneath a Thick Turbulent Boundary Layer. J. Fluid Mech., vol. 14, 1962, p. 187.

13. Lilley, G. M.: Wall Pressure Fluctuations Under Turbulent Boundary Layer at Subsonic and Supersonic Speeds. AGARD Rep. 454, April 1963.

14. Belcher, P. M.: Predictions of Boundary-Layer-Turbulence Spectra and Correlations for Supersonic Flight. 5^{e} Congres International D'Acoustique, Liege, Sept. 1965.

15. Williams, D. J. M.: Measurements of the Surface Pressure Fluctuations in a Turbulent Boundary Layer in Air at Supersonic Speeds. A.A.S.U. Rep. 162, Dec. 1965.

16. Kister, A. L.; and Chen, W. S.: The Fluctuating Pressure Field in a Supersonic Turbulent Boundary Layer. J. Fluid Mech., vol. 16, pt. 1, 1963, p. 41.

17. Speaker, W. F.; and Ailman, C. M.: Spectra and Space-Time Correlations of the Fluctuating Pressures at a Wall Beneath a Supersonic Turbulent Boundary Layer Perturbed by Steps and Shock Waves. Douglas Rep. SM-49806, Nov. 1965.

18. Kistler, A. L.: Fluctuating Wall Pressure Under a Separated Supersonic Flow. J. ASA, vol. 36, no. 3, March 1964, p. 543.

19. Allen, J. M.; and Monta, W. J.: Turbulent-Boundary-Layer Characteristics of Pointed Slender Bodies of Revolution at Supersonic Speeds. NASA TN D-4193, 1967.

20. Corcos, G. M.; Cuthbert, J. W.; and von Winkle, W. A.: On the Measurement of Turbulent Pressure Fluctuations With a Transducer of Finite Size. University of California Institute of Engineering Research Rep., Ser. 82, Issue 20, Sept. 1961.

21. Lim, R. S.; and Cameron, W. D.: Power and Cross-Power Spectrum Analysis by Hybrid Computer. NASA TM X-1324, 1966.

22. Bendat, J. S.; and Piersol, A. G.: Measurement and Analysis of Random Data. John Wiley and Sons, Inc., 1966.

23. Chapman, D. R.; Kuehn, D. M; and Larson, H. K.: Investigation of Separated Flows in Supersonic and Subsonic Streams With Emphasis on the Effect of Transition. NACA TR-1356, 1958.